

Non-Hermitian Mott Skin Effect

Tsuneya Yoshida,¹ Song-Bo Zhang,² Titus Neupert,³ and Norio Kawakami^{1,4,5}

¹*Department of Physics, Kyoto University, Kyoto 606-8502, Japan*

²*International Center for Quantum Design of Functional Materials (ICQD),*

Hefei National Research Center for Physical Sciences at the Microscale,

University of Science and Technology of China, Hefei, Anhui 230026, China

³*Department of Physics, University of Zürich, Winterthurerstrasse 190, 8057, Zürich, Switzerland*

⁴*Department of Materials Engineering Science, Osaka University, Toyonaka 560-8531, Japan*

⁵*Department of Physics, Ritsumeikan University, Kusatsu, Shiga 525-8577, Japan*

(Dated: October 2, 2023)

We propose a novel type of skin effects in non-Hermitian quantum many-body systems which we dub a non-Hermitian Mott skin effect. This phenomenon is induced by the interplay between strong correlations and the non-Hermitian point-gap topology. The Mott skin effect induces extreme sensitivity to the boundary conditions only in the spin degree of freedom (i.e., the charge distribution is not sensitive to boundary conditions), which is in sharp contrast to the ordinary non-Hermitian skin effect in non-interacting systems. Concretely, we elucidate that a bosonic non-Hermitian chain exhibits the Mott skin effect in the strongly correlated regime by closely examining an effective Hamiltonian. The emergence of the Mott skin effect is also supported by numerical diagonalization of the bosonic chain. The difference between the ordinary non-Hermitian skin effect and the Mott skin effect is also reflected in the time-evolution of physical quantities; under the time-evolution spin accumulation is observed while the charge distribution remains spatially uniform.

Introduction-. Since the discovery of topological insulators, extensive efforts have been devoted to understanding topological aspects of condensed matter systems [1–9]. While topological insulators are originally reported for free fermions, it has turned out that the interplay between strong correlations and non-trivial topology triggers further exotic phenomena [10–33]. For instance, strong correlations can induce fractional quantum Hall states [10, 11, 15, 21–26]. Furthermore, topological Mott insulators exhibit the unique bulk-edge correspondence due to the interplay between correlations and the non-trivial topology [34–36]. Namely, corresponding to the non-trivial topology in the bulk, gapless edge modes emerge only in the spin excitation spectrum (i.e., the charge excitation spectrum is gapped even around edges).

Along with the above progress, the topological band theory of non-Hermitian systems has been developed [37–67] and revealed unique phenomena due to the non-Hermitian point-gap topology which do not have Hermitian counterparts [68–82]. A representative example is the non-Hermitian skin effect [83–105] which results in the novel bulk-edge correspondence unique to non-Hermitian systems; because of the non-trivial point-gap topology in the bulk, the eigenstates and eigenvalues exhibit extreme sensitivity to the presence or absence of boundaries [91, 92]. Especially, in one-dimensional systems, most of eigenstates are localized only around one of the edges under open boundary conditions (OBC), while eigenstates extend to the bulk under periodic boundary conditions (PBC). The above localized eigenstates are known as skin modes.

The above progress on correlated systems and the non-interacting non-Hermitian topology naturally leads us to the following crucial question: *how do strong corre-*

lations affect the non-Hermitian skin effects? The significance of this issue is further enhanced by recent advances in experiments with cold atoms [106–108] and quantum circuits [109] where both dissipation and correlations can be introduced. Correlation effects on the non-Hermitian topological properties have been studied extensively [110–140], but not on non-Hermitian skin effects, which is particularly the case for bosonic systems.

In this paper, we address this question for a one-dimensional bosonic system and discover a novel type of skin effects, a *non-Hermitian Mott skin effect*, which induces striking skin modes. Namely, the non-trivial point-gap topology results in the skin modes in which only the spin degree of freedom is involved (i.e., charges are distributed uniformly even under OBC). This behavior is in sharp contrast to non-Hermitian skin effects in non-interacting systems where bosons are localized around the edge. We elucidate the emergence of the Mott skin effect by examining an effective spin model in the strong correlation regime, which hosts skin modes and possesses the non-trivial point-gap topology characterized by the spin winding number. We also support the emergence of the Mott skin effect by employing numerical diagonalization. Our numerical analysis also elucidates unique real-time dynamics induced by the Mott skin effect; dynamical spin accumulation is observed while the charge distribution remains spatially uniform.

Model-. Let us consider a one-dimensional chain of

interacting bosons. The Hamiltonian reads

$$\hat{H} = \hat{H}_0 + \hat{H}_{\text{int}}, \quad (1)$$

$$\hat{H}_0 = \sum_{j\sigma} (-t_{R\sigma} \hat{b}_{j+1\sigma}^\dagger \hat{b}_{j\sigma} - t_{L\sigma} \hat{b}_{j\sigma}^\dagger \hat{b}_{j+1\sigma}), \quad (2)$$

$$\hat{H}_{\text{int}} = -iV \sum_{j\sigma} \hat{n}_{j\sigma} (\hat{n}_{j\sigma} - 1) - iU \sum_j \hat{n}_{j\uparrow} \hat{n}_{j\downarrow}, \quad (3)$$

where $\hat{b}_{j\sigma}^\dagger$ ($\hat{b}_{j\sigma}$) creates (annihilates) a boson at site $j = 0, 1, 2, \dots, L-1$ and in the spin state $\sigma = \uparrow, \downarrow$ [141]. The non-reciprocal hopping integrals are denoted by $t_{R\uparrow} = t_{L\downarrow} = t_+$ and $t_{L\uparrow} = t_{R\downarrow} = t_-$ with real numbers t_+ and t_- . The operator $\hat{n}_{j\sigma}$ denotes the number operator of bosons of spin σ at site j ; $\hat{n}_{j\sigma} := \hat{b}_{j\sigma}^\dagger \hat{b}_{j\sigma}$. The first (second) term of \hat{H}_{int} describes the on-site interaction between bosons with the same (opposite) spin. The parameters V and U are non-negative numbers. Throughout this paper, we suppose the relation $t_+ > t_-$.

Symmetry and a topological invariant. The above model preserves charge U(1) symmetry and spin U(1) symmetry

$$[\hat{H}, \hat{N}] = 0, \quad (4)$$

$$[\hat{H}, \hat{S}^z] = 0, \quad (5)$$

with $\hat{N} = \hat{N}_\uparrow + \hat{N}_\downarrow$ and $2\hat{S}^z = \hat{N}_\uparrow - \hat{N}_\downarrow$. Here, \hat{N}_σ denotes the number operator of bosons in the spin state σ ; $\hat{N}_\sigma = \sum_j \hat{n}_{j\sigma}$ ($\sigma = \uparrow, \downarrow$). Therefore, the Hamiltonian can be block-diagonalized into N_\uparrow and N_\downarrow sectors. We denote eigenvalues of \hat{N}_\uparrow and \hat{N}_\downarrow as N_\uparrow and N_\downarrow , respectively.

In order to characterize the point-gap topology [142], we introduce the many-body spin winding number

$$W_s = \int_0^{2\pi} \frac{d\theta_s}{2\pi i} \frac{\partial}{\partial \theta_s} \log \left[\det \left(\hat{H}_{[N_\uparrow, N_\downarrow]}(\theta_s) - E_{\text{ref}} \right) \right] \quad (6)$$

which is a variant of the previously introduced many-body winding number [125, 131, 132]. Here, in order to compute W_s , we have imposed twisted boundary conditions where the twist angle of the down-spin state θ_\downarrow is opposite to that of the up-spin state θ_\uparrow [143]; $\hat{b}_{0\sigma}^\dagger \hat{b}_{L-1\sigma} \rightarrow e^{i\theta_\sigma} \hat{b}_{0\sigma}^\dagger \hat{b}_{L-1\sigma}$ with $(\theta_\uparrow, \theta_\downarrow) = (\theta_s, -\theta_s)$ and the twist angle θ_s . For the Fock space specified by $[N_\uparrow, N_\downarrow]$, the block-diagonalized Hamiltonian is denoted by $\hat{H}_{[N_\uparrow, N_\downarrow]}(\theta_s)$.

Analysis in the strong coupling region. Before presenting numerical results, we derive an effective model which provides an intuition for the Mott skin effect. In the strong coupling region (i.e., $V, U \gg t_+, t_-$), longest lived states of the system are described by an effective spin model, i.e., eigenstates shift in the negative direction of the imaginary axis if bosons occupy the same site. Applying the second order perturbation theory yields the following effective spin model for the states where each

site is occupied by one boson

$$\begin{aligned} \hat{H}_{\text{spin}}(\theta_s) = & \sum_{j=0}^{L-2} \left[J_z \hat{S}_{j+1}^z \hat{S}_j^z + J_+ \hat{S}_{j+1}^+ \hat{S}_j^- + J_- \hat{S}_{j+1}^- \hat{S}_j^+ \right] \\ & + J_+ e^{2i\theta_s} \hat{S}_0^+ \hat{S}_{L-1}^- + J_- e^{-2i\theta_s} \hat{S}_0^- \hat{S}_{L-1}^+ + E_0, \end{aligned} \quad (7)$$

with $J_z = -4i(t_+ t_-)(\frac{1}{V} - \frac{1}{U})$, $J_\pm = -2i\frac{t_\pm^2}{U}$, and $E_0 = -iL(t_+ t_-)(\frac{1}{V} + \frac{1}{U})$. Here, \hat{S}_j^μ ($\mu = x, y, z$) denotes spin operators at site j . The spin raising and lowering operators are defined as $\hat{S}_j^\pm = \hat{S}_j^x \pm i\hat{S}_j^y$. In terms of creation and annihilation operators of bosons, the spin operators are written as $\hat{S}_j^z = (\hat{n}_{j\uparrow} - \hat{n}_{j\downarrow})/2$, $\hat{S}_j^+ = \hat{b}_{j\uparrow}^\dagger \hat{b}_{j\downarrow}$ and $\hat{S}_j^- = \hat{b}_{j\downarrow}^\dagger \hat{b}_{j\uparrow}$ for the subspace where each site is occupied by one boson. Details of the derivation are provided in Sec. S1 of Supplemental Material [144]. The above Hamiltonian (7) preserves spin U(1) symmetry and can be block-diagonalized with S^z , the eigenvalue of $\hat{S}^z = \sum_j \hat{S}_j^z$.

Applying the Jordan-Wigner transformation elucidates that the effective model (7) gives rise to the Mott skin effect (for the detailed derivation, see Sec. S1 of Supplemental Material [144]); the spin model [Eq. (7)] can be mapped to the following spinless fermion model

$$\begin{aligned} \hat{H}_{\text{spin}}(\theta) = & \sum_{j=0}^{L-2} \left(J_+ \hat{f}_{j+1}^\dagger \hat{f}_j + J_- \hat{f}_j^\dagger \hat{f}_{j+1} \right) \\ & - (-1)^{N^f} \left(J_+ e^{2i\theta_s} \hat{f}_0^\dagger \hat{f}_{L-1} + J_- e^{-2i\theta_s} \hat{f}_{L-1}^\dagger \hat{f}_0 \right) \\ & + J_z \sum_{j=0}^{L-1} \hat{n}_{j+1}^f \hat{n}_j^f - J_z \left(N^f - \frac{L}{4} \right) + E_0, \end{aligned} \quad (8)$$

with $N^f = \sum_j \hat{n}_j^f$, $\hat{S}_j^+ = e^{i\pi \hat{N}_j^<} \hat{f}_j^\dagger$, and $\hat{S}_j^z = (\hat{n}_j^f - \frac{1}{2})$. Here, $\hat{N}_j^<$ and \hat{n}_j^f are defined as $\hat{N}_j^< = \sum_{k=0}^{j-1} \hat{n}_k^f$ and $\hat{n}_j^f = \hat{f}_j^\dagger \hat{f}_j$. Operators \hat{f}_j^\dagger (\hat{f}_j) create (annihilate) a spinless fermion at site j .

In particular, for the subspace with $S^z = 1 - \frac{L}{2}$ (i.e., $[N_\uparrow, N_\downarrow] = [1, L-1]$), there exists only one fermion created by \hat{f}_j^\dagger . Therefore, the above Hamiltonian is simplified as

$$\begin{aligned} \hat{H}_{\text{spin}}(\theta) = & \sum_{j=0}^{L-2} \left(J_+ \hat{f}_{j+1}^\dagger \hat{f}_j + J_- \hat{f}_j^\dagger \hat{f}_{j+1} \right) \\ & + \left(J_+ e^{2i\theta_s} \hat{f}_0^\dagger \hat{f}_{L-1} + J_- e^{-2i\theta_s} \hat{f}_{L-1}^\dagger \hat{f}_0 \right) \\ & + J_z \left(\frac{L}{4} - 1 \right) + E_0. \end{aligned} \quad (9)$$

This model is nothing but the Hatano-Nelson chain [44, 45] which exhibits the skin effect. Specifically, substituting the Hamiltonian (9) to $\hat{H}_{[1, L-1]}(\theta_s)$, we obtain the winding number $W_s = 2$ for the subspace with

$[N_\uparrow, N_\downarrow] = [1, L - 1]$. Here, we have set the reference energy E_{ref} located inside of the loop formed by the eigenvalues. We recall that $iJ_+ > iJ_-$ holds for $t_+ > t_-$ [see below Eq. (7)]. Corresponding to this non-trivial point-gap topology, skin modes emerge only around the right edge which are described by fermions created by \hat{f}_j^\dagger . We note that the eigenvalues are aligned on the imaginary axis because J_+ and J_- are purely imaginary [145].

Recalling the relation between spin operators and operators \hat{f}_j^\dagger , we can conclude that the system exhibits the Mott skin effect. Namely, only the spin degree of freedom is involved in the skin modes induced by the non-trivial point-gap topology.

Numerical results: non-interacting case-. In order to numerically analyze this model, we employ exact diagonalization. Unless otherwise noted, we set $(t_+, t_-) = (1, 0.1)$.

In the non-interacting case, the system is decomposed into two bosonic Hatano-Nelson models where the hopping in the right (left) direction is dominant for $\sigma = \uparrow$ ($\sigma = \downarrow$). Such non-reciprocal hoppings result in the ordinary non-Hermitian skin effect as discussed below. In the following, we analyze the many-body Hamiltonian (1) for the Fock space with $(N_\uparrow, N_\downarrow) = (1, L - 1)$ with $L = 6$ (for analysis of the one-body Hamiltonian, see Sec. S2 of Supplemental Material [144]).

Figure 1(a) displays the spectral flow of $\hat{H}(\theta_s)$ for $0 \leq \theta_s \leq 2\pi$ where $E_m(\theta_s)$ ($m = 0, 1, 2, \dots$) are eigenvalues of $\hat{H}(\theta_s)$. In this figure, we can see that the spectral flow forms the loop structure, which indicates the point-gap topology characterized by the many-body spin winding number taking a non-zero value for $E_{\text{ref}} = -0.01i$ (for more details, see Sec. S3 of Supplemental Material [144]).

Corresponding to this non-trivial point-gap topology, the spectrum shows extreme sensitivity to the boundary conditions. Imposing OBC significantly changes the spectrum of \hat{H} ; as shown in Fig. 1(a) the eigenvalues under OBC are aligned on the real axis in contrast to the eigenvalues under PBC. Eigenstates also show such sensitivity to the boundary conditions [146]. In order to show this, we compute the expectation values of $\hat{n}_j = \sum_\sigma \hat{n}_{j\sigma}$

$$\langle \hat{n}_j \rangle = \frac{\text{R}\langle \Psi_m | \hat{n}_j | \Psi_m \rangle_{\text{R}}}{\text{R}\langle \Psi_m | \Psi_m \rangle_{\text{R}}}, \quad (10)$$

with $|\Psi_m\rangle_{\text{R}}$ ($m = 0, 1, 2, \dots$) being right eigenvectors of the many-body Hamiltonian, $\hat{H}|\Psi_m\rangle_{\text{R}} = E_m|\Psi_m\rangle_{\text{R}}$. As displayed in Fig. 1(c), bosons are localized around edges under OBC in contrast to the case of PBC (the data for PBC is provided in Sec. S4 of Supplemental Material [144]).

Due to the localization of bosons, spin polarization is observed only in the presence of boundaries. Figure 1(c) displays the expectation values of $\hat{S}_j^z = (\hat{n}_{j\uparrow} - \hat{n}_{j\downarrow})/2$. Spin polarization is observed under OBC in contrast to the case of PBC.

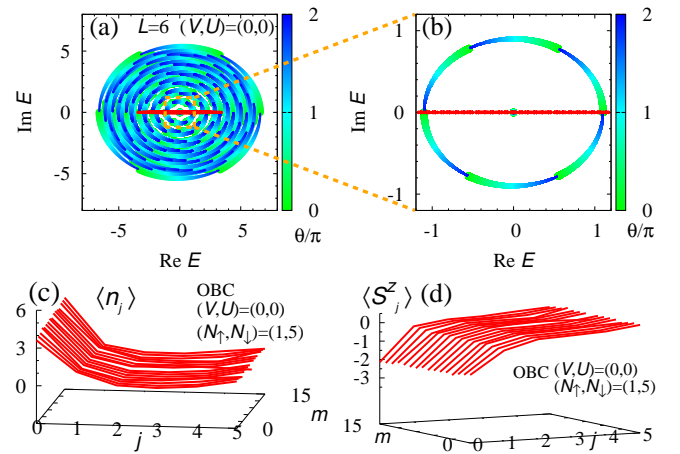


FIG. 1. Energy eigenvalues and expectation values for $V = U = 0$. (a): Energy eigenvalues under twisted boundary conditions and OBC (red), respectively. (b): A magnified version of the range $-1.2 \leq \text{Im}E \leq 1.2$. The data obtained under OBC are represented by red dots. With increasing θ_s from 0 to 2π , the eigenvalues wind the origin of the complex plane, which indicates W_s takes a non-zero value for $E_{\text{ref}} = -0.01i$. (c) [(d)]: Expectation values $\langle \hat{n}_j \rangle$ [$\langle \hat{S}_j^z \rangle$] at each site under OBC. Here, the expectation values are computed from right eigenvectors of the many-body Hamiltonian labeled by m [see Eq. (10)]. These data are obtained for subspace with $(N_\uparrow, N_\downarrow) = (1, 5)$ and for $(t_+, t_-) = (1, 0.1)$ and $L = 6$.

As discussed above, in the non-interacting cases, the system shows the non-Hermitian skin effect which results in extreme sensitivity of the eigenvalues and eigenstates to the presence or absence of the boundaries. Accordingly, the localization of bosons is observed only under OBC.

Numerical results: interacting case-. Now, we demonstrate that the interplay between strong correlations and non-reciprocal hoppings induces the Mott skin effect. Namely, the non-trivial point-gap topology results in extreme sensitivity to the boundary conditions only in the spin degree of freedom. The spin-charge separation plays an essential role in the emergence of the Mott skin effect. In the following, we focus on the Fock space with $(N_\uparrow, N_\downarrow) = (1, L - 1)$ [147].

Figures 2(a) and 2(b) display the spectral flow of $\hat{H}(\theta_s)$ for $(V, U) = (100, 20)$ with increasing θ_s from 0 to 2π . The interactions V and U shift most of the loops in the negative direction of the imaginary axis [see Fig. 2(a)]. However, one of the loops remains around the origin of the complex plane [see Fig. 2(b)]. This is because bosons do not feel the on-site interactions unless multiple bosons occupy the same site.

The states remaining around the origin of the complex plane exhibit the Mott skin effect. Because of the loop structure, the many-body spin winding number takes $W_s = 2$ for $E_{\text{ref}} = -0.01i$ (for more details, see Sec. S3 of

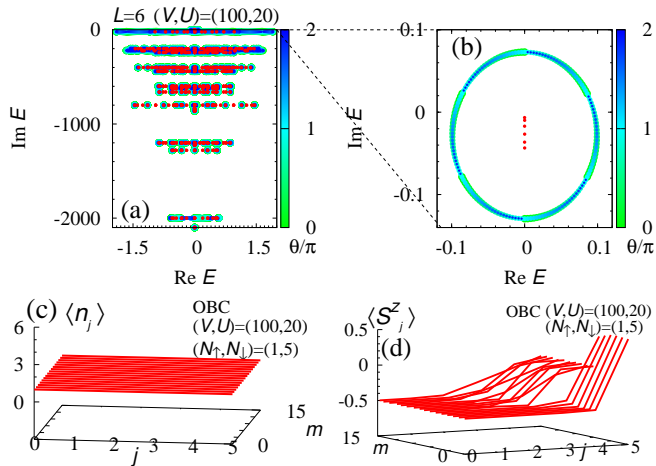


FIG. 2. Energy eigenvalues and expectation values for $(V, U) = (100, 20)$. (a): Energy eigenvalues under twisted boundary conditions and OBC, respectively. (b): A magnified version of the range $-0.14 \leq \text{Im}E \leq 0.1$. In these figures the data obtained under OBC are represented by red dots. With increasing θ_s from 0 to 2π , the eigenvalues wind the origin of the complex plane, which indicates $W_s = 2$ for $E_{\text{ref}} = -0.01i$. (c) [(d)]: Expectation values $\langle \hat{n}_j \rangle$ [$\langle \hat{S}_j^z \rangle$] at each site under OBC. As is the case of $V = U = 0$, the expectation values are computed from the right eigenvectors (see Fig. 1). These data are obtained for $(t_+, t_-) = (1, 0.1)$ and $L = 6$.

Supplemental Material [144]). Corresponding to the non-trivial point-gap topology, eigenstates exhibit extreme sensitivity to the presence or absence of the boundaries. As shown in Fig. 2(b), the eigenvalues are aligned on the imaginary axis under OBC in contrast to the case of PBC where eigenvalues are distributed on the complex plane [148].

Such sensitivity to the boundary conditions is also observed for eigenstates. However, only the spin degree of freedom is involved in the sensitivity of the boundary conditions, which is in sharp contrast to the non-interacting case. Figure 2(c) displays the expectation values $\langle \hat{n}_j \rangle$. As shown in this figure, strong correlations prevent bosons from localizing around the edges, which suppresses the sensitivity to the boundary conditions for the charge degree of freedom. Instead, the spin degree of freedom exhibits extreme sensitivity to the boundary conditions. Figure 2(d) displays the expectation values $\langle \hat{S}_j^z \rangle$. As shown in this figure, spin polarization is observed under OBC in contrast to the case of PBC (the data for PBC are provided in Sec. S4 of Supplemental Material [144]).

The above results reveal that the system exhibits the Mott skin effect resulting in extreme sensitivity to the boundary conditions only in the spin degree of freedom (i.e., such sensitivity is not observed in the charge degree of freedom). The emergence of the Mott skin effect is due to the interplay between strong correlations

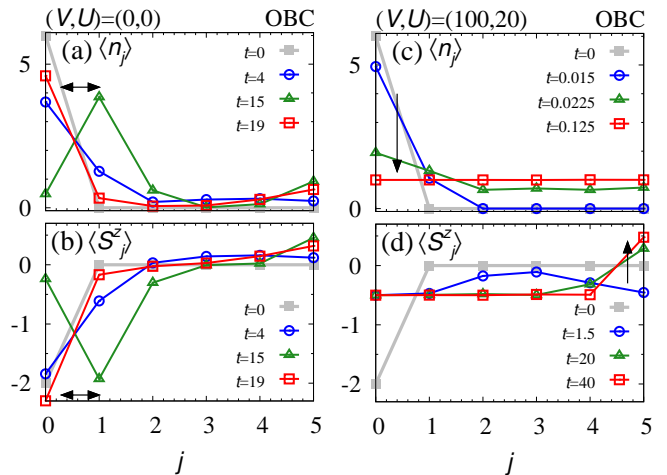


FIG. 3. (a) and (c) [(b) and (d)]: The time-evolution of the expectation values $\langle \hat{n}_j(t) \rangle$ [$\langle \hat{S}_j^z(t) \rangle$] under OBC [see Eq. (11)]. Panels (a) and (b) [(c) and (d)] display data for $(V, U) = (0, 0)$ [$(V, U) = (100, 20)$]. These data are obtained for $(t_+, t_-) = (1, 0.1)$ and $L = 6$.

and non-Hermitian point-gap topology. We note that the Mott skin effect is observed also for the subspace with $(N_\uparrow, N_\downarrow) = (2, 4)$ and $L = 6$ (for more details see Sec. S5 of Supplemental Material [144]).

Real-time dynamics-. As seen above, the Mott skin effect involves only the spin degree of freedom in contrast to the skin effect in the non-interacting case. This difference is also reflected in the time-evolution of physical quantities.

Let us start with the non-interacting case. Figure 3(a) displays the expectation values

$$\langle \hat{n}_j(t) \rangle = \frac{\langle \Phi(t) | \hat{n}_j | \Phi(t) \rangle}{\langle \Phi(t) | \Phi(t) \rangle}, \quad (11)$$

with $|\Phi(t)\rangle = e^{-i\hat{H}t}|\Phi(0)\rangle$ and t being time [149]. The initial state is chosen so that all of the bosons occupy site $j = 0$; $\sqrt{(L-1)!}|\Phi(0)\rangle = \hat{b}_{0\uparrow}^\dagger (\hat{b}_{0\downarrow}^\dagger)^{L-1}|0\rangle$. Figure 3(a) indicates that the bosons remain localized around the left edge due to the skin effect [150]. Figure 3(b) indicates that the above localization is also observed in the expectation values $\langle \hat{S}_j^z(t) \rangle = \langle \Phi(t) | \hat{S}_j^z | \Phi(t) \rangle / \langle \Phi(t) | \Phi(t) \rangle$. This is because bosons with spin up (spin down) are localized around the right (left) edge (see Sec. S2 of Supplemental Material [144]). The above results demonstrate that in the non-interacting case, the dynamical properties of the spin degree of freedom are tied to those of charge degree of freedom.

Now, we turn to the real-time dynamics in the correlated case. In contrast to the non-interacting case, dynamics of the spin degree of freedom exhibit an essential difference from those of the charge degree of freedom. Figure 3(c) displays the time-evolution of $\langle \hat{n}_j(t) \rangle$ for $(V, U) = (100, 20)$. As seen in Fig. 3(c), bosons immediately extend to the bulk. In particular, for $0.125 \lesssim t$,

each site is occupied by one boson. This is because the states where each site is occupied by one boson have a longer lifetime $\tau \sim 1/\text{Im}E_m$ than others. Contrary to the sudden change in the charge degree of freedom, the dynamics of the spin degree of freedom show gradual changes. The time-evolution of $\langle \hat{S}_j^z \rangle$ is plotted in Fig. 3(d). In this figure, dynamical spin accumulation is observed for $20 \lesssim t$. This behavior is observed only under OBC (for data under PBC, see Sec. S6 of Supplemental Material [144]).

As seen above, the Mott skin effect induces the dynamical spin accumulation while the charge degree of freedom remains spatially uniform. These dynamical properties in the strongly correlated case are in sharp contrast to those in the non-interacting case. The above dynamical properties are considered to be observed for open quantum systems even in the presence of quantum jumps.

Conclusion–. We have proposed a non-Hermitian Mott skin effect induced by the interplay between strong correlations and the non-Hermitian point-gap topology. In contrast to the ordinary non-Hermitian skin effect, the Mott skin effect results in extreme sensitivity to the boundary conditions only in the spin degree of freedom. We have demonstrated the emergence of the Mott skin effect by analyzing the bosonic non-Hermitian Hamiltonian with non-reciprocal hoppings and on-site interactions. The difference from the ordinary skin effect is also reflected in the dynamical properties; spin accumulation is observed while charge distribution remains spatially uniform.

We finish this paper with a remark on the relevance to open quantum systems described by the Lindblad equation. In this paper, we have analyzed the non-Hermitian Hamiltonian as a toy model. However, we argue that our Hamiltonian is relevant to open quantum systems, and that the above dynamical spin accumulation can be observed even under the presence of the jump term.

Note added–. While finishing this paper, we noticed Ref. [151] posted on arXiv which has some overlap with our results.

Acknowledgments–. T.Y. thanks Manfred Sigrist for fruitful discussion. T.Y. particularly thanks Shunsuke Furukawa and Yoshihito Kuno for fruitful discussions on the technical details of exact diagonalization. T.Y. is grateful to the long term workshop YITP-T-23-01 held at YITP, Kyoto University, where a part of this work was done. This work is supported by JSPS KAKENHI Grants No. JP21K13850 and No. JP22H05247.

[1] M. Z. Hasan and C. L. Kane, *Rev. Mod. Phys.* **82**, 3045 (2010).
 [2] X.-L. Qi and S.-C. Zhang, *Rev. Mod. Phys.* **83**, 1057 (2011).

[3] D. J. Thouless, M. Kohmoto, M. P. Nightingale, and M. den Nijs, *Phys. Rev. Lett.* **49**, 405 (1982).
 [4] B. I. Halperin, *Phys. Rev. B* **25**, 2185 (1982).
 [5] Y. Hatsugai, *Phys. Rev. Lett.* **71**, 3697 (1993).
 [6] A. Y. Kitaev, *Physics-Uspekhi* **44**, 131 (2001).
 [7] C. L. Kane and E. J. Mele, *Phys. Rev. Lett.* **95**, 146802 (2005).
 [8] C. L. Kane and E. J. Mele, *Phys. Rev. Lett.* **95**, 226801 (2005).
 [9] X.-L. Qi, T. L. Hughes, and S.-C. Zhang, *Phys. Rev. B* **78**, 195424 (2008).
 [10] D. C. Tsui, H. L. Stormer, and A. C. Gossard, *Phys. Rev. Lett.* **48**, 1559 (1982).
 [11] R. B. Laughlin, *Phys. Rev. Lett.* **50**, 1395 (1983).
 [12] J. K. Jain, *Phys. Rev. Lett.* **63**, 199 (1989).
 [13] F. D. M. Haldane, *Phys. Rev. Lett.* **51**, 605 (1983).
 [14] F. D. M. Haldane, *Phys. Rev. Lett.* **55**, 2095 (1985).
 [15] X.-G. Wen, *Advances in Physics* **44**, 405 (1995).
 [16] *Annals of Physics* **303**, 2 (2003).
 [17] X.-G. Wen, *Quantum field theory of many-body systems: from the origin of sound to an origin of light and electrons* (OUP Oxford, 2004).
 [18] M. A. Levin and X.-G. Wen, *Phys. Rev. B* **71**, 045110 (2005).
 [19] A. Kitaev, *Annals of Physics* **303**, 2 (2003).
 [20] A. Kitaev, *Annals of Physics* **321**, 2 (2006), January Special Issue.
 [21] E. Tang, J.-W. Mei, and X.-G. Wen, *Phys. Rev. Lett.* **106**, 236802 (2011).
 [22] K. Sun, Z. Gu, H. Katsura, and S. Das Sarma, *Phys. Rev. Lett.* **106**, 236803 (2011).
 [23] T. Neupert, L. Santos, C. Chamon, and C. Mudry, *Phys. Rev. Lett.* **106**, 236804 (2011).
 [24] D. N. Sheng, Z.-C. Gu, K. Sun, and L. Sheng, *Nature Communications* **2**, 389 EP (2011), article.
 [25] N. Regnault and B. A. Bernevig, *Phys. Rev. X* **1**, 021014 (2011).
 [26] E. J. Bergholtz and Z. Liu, *International Journal of Modern Physics B* **27**, 1330017 (2013).
 [27] L. Fidkowski and A. Kitaev, *Phys. Rev. B* **81**, 134509 (2010).
 [28] A. M. Turner, F. Pollmann, and E. Berg, *Phys. Rev. B* **83**, 075102 (2011).
 [29] L. Fidkowski and A. Kitaev, *Phys. Rev. B* **83**, 075103 (2011).
 [30] Z.-C. Gu and X.-G. Wen, *Phys. Rev. B* **90**, 115141 (2014).
 [31] H. Yao and S. Ryu, *Phys. Rev. B* **88**, 064507 (2013).
 [32] S. Ryu and S.-C. Zhang, *Phys. Rev. B* **85**, 245132 (2012).
 [33] X.-L. Qi, *New J. Phys.* **15**, 065002 (2013).
 [34] D. Pesin and L. Balents, *Nature Physics* **6**, 376 (2010).
 [35] S. R. Manmana, A. M. Essin, R. M. Noack, and V. Gurarie, *Phys. Rev. B* **86**, 205119 (2012).
 [36] T. Yoshida, R. Peters, S. Fujimoto, and N. Kawakami, *Phys. Rev. Lett.* **112**, 196404 (2014).
 [37] E. J. Bergholtz, J. C. Budich, and F. K. Kunst, *Rev. Mod. Phys.* **93**, 015005 (2021).
 [38] Y. Ashida, Z. Gong, and M. Ueda, *Advances in Physics* **69**, 249 (2020).
 [39] Z. Gong, Y. Ashida, K. Kawabata, K. Takasan, S. Higashikawa, and M. Ueda, *Phys. Rev. X* **8**, 031079 (2018).
 [40] K. Kawabata, S. Higashikawa, Z. Gong, Y. Ashida, and

- M. Ueda, *Nature Communications* **10**, 297 (2019).
- [41] K. Kawabata, K. Shiozaki, M. Ueda, and M. Sato, *Phys. Rev. X* **9**, 041015 (2019).
- [42] H. Zhou and J. Y. Lee, *Phys. Rev. B* **99**, 235112 (2019).
- [43] S. Lieu, M. McGinley, and N. R. Cooper, *Phys. Rev. Lett.* **124**, 040401 (2020).
- [44] N. Hatano and D. R. Nelson, *Phys. Rev. Lett.* **77**, 570 (1996).
- [45] N. Hatano and D. R. Nelson, *Phys. Rev. B* **56**, 8651 (1997).
- [46] C. M. Bender and S. Boettcher, *Phys. Rev. Lett.* **80**, 5243 (1998).
- [47] T. Fukui and N. Kawakami, *Physical Review B* **58**, 16051 (1998).
- [48] Y. Ashida, S. Furukawa, and M. Ueda, *Phys. Rev. A* **94**, 053615 (2016).
- [49] Y. C. Hu and T. L. Hughes, *Phys. Rev. B* **84**, 153101 (2011).
- [50] K. Esaki, M. Sato, K. Hasebe, and M. Kohmoto, *Phys. Rev. B* **84**, 205128 (2011).
- [51] M. Sato, K. Hasebe, K. Esaki, and M. Kohmoto, *Progress of Theoretical Physics* **127**, 937 (2012).
- [52] S. Diehl, E. Rico, M. A. Baranov, and P. Zoller, *Nature Physics* **7**, 971 (2011).
- [53] C.-E. Bardyn, M. A. Baranov, C. V. Kraus, E. Rico, A. İmamoğlu, P. Zoller, and S. Diehl, *New Journal of Physics* **15**, 085001 (2013).
- [54] A. Rivas, O. Viyuela, and M. A. Martin-Delgado, *Phys. Rev. B* **88**, 155141 (2013).
- [55] B. Zhu, R. Lü, and S. Chen, *Phys. Rev. A* **89**, 062102 (2014).
- [56] J. C. Budich, P. Zoller, and S. Diehl, *Phys. Rev. A* **91**, 042117 (2015).
- [57] S. Lieu, *Phys. Rev. B* **97**, 045106 (2018).
- [58] W. B. Rui, Y. X. Zhao, and A. P. Schnyder, *Phys. Rev. B* **99**, 241110 (2019).
- [59] M. M. Denner, A. Skurativska, F. Schindler, M. H. Fischer, R. Thomale, T. Bzdusek, and T. Neupert, *Nature Communications* **12** (2021).
- [60] D. Nakamura, T. Bessho, and M. Sato, arXiv preprint arXiv:2205.15635 (2022).
- [61] K. Yokomizo and S. Murakami, *Phys. Rev. Lett.* **123**, 066404 (2019).
- [62] K. Kawabata, N. Okuma, and M. Sato, *Phys. Rev. B* **101**, 195147 (2020).
- [63] F. Tonielli, J. C. Budich, A. Altland, and S. Diehl, *Phys. Rev. Lett.* **124**, 240404 (2020).
- [64] K. Kawabata, K. Shiozaki, and S. Ryu, *Phys. Rev. Lett.* **126**, 216405 (2021).
- [65] S. Sayyad, J. D. Hannukainen, and A. G. Grushin, *Phys. Rev. Res.* **4**, L042004 (2022).
- [66] P.-Y. Chang, J.-S. You, X. Wen, and S. Ryu, *Phys. Rev. Res.* **2**, 033069 (2020).
- [67] C.-T. Hsieh and P.-Y. Chang, *SciPost Phys. Core* **6**, 062 (2023).
- [68] H. Shen, B. Zhen, and L. Fu, *Phys. Rev. Lett.* **120**, 146402 (2018).
- [69] V. Kozii and L. Fu, arXiv preprint arXiv:1708.05841 (2017).
- [70] T. Yoshida, R. Peters, and N. Kawakami, *Phys. Rev. B* **98**, 035141 (2018).
- [71] H. Zhou, C. Peng, Y. Yoon, C. W. Hsu, K. A. Nelson, L. Fu, J. D. Joannopoulos, M. Soljačić, and B. Zhen, *Science* **359**, 1009 (2018).
- [72] Z. Yang, A. P. Schnyder, J. Hu, and C.-K. Chiu, *Phys. Rev. Lett.* **126**, 086401 (2021).
- [73] J. C. Budich, J. Carlström, F. K. Kunst, and E. J. Bergholtz, *Phys. Rev. B* **99**, 041406 (2019).
- [74] R. Okugawa and T. Yokoyama, *Phys. Rev. B* **99**, 041202 (2019).
- [75] H. Zhou, J. Y. Lee, S. Liu, and B. Zhen, *Optica* **6**, 190 (2019).
- [76] T. Yoshida, R. Peters, N. Kawakami, and Y. Hatsugai, *Phys. Rev. B* **99**, 121101 (2019).
- [77] T. Yoshida, R. Peters, N. Kawakami, and Y. Hatsugai, *Progress of Theoretical and Experimental Physics* **2020**, 12A109 (2020).
- [78] K. Kawabata, T. Bessho, and M. Sato, *Phys. Rev. Lett.* **123**, 066405 (2019).
- [79] J. Carlström, M. Stålhammar, J. C. Budich, and E. J. Bergholtz, *Phys. Rev. B* **99**, 161115 (2019).
- [80] Y. Xu, S.-T. Wang, and L.-M. Duan, *Phys. Rev. Lett.* **118**, 045701 (2017).
- [81] P. Delplace, T. Yoshida, and Y. Hatsugai, *Phys. Rev. Lett.* **127**, 186602 (2021).
- [82] I. Mandal and E. J. Bergholtz, *Phys. Rev. Lett.* **127**, 186601 (2021).
- [83] T. E. Lee, *Phys. Rev. Lett.* **116**, 133903 (2016).
- [84] V. M. Martinez Alvarez, J. E. Barrios Vargas, and L. E. F. Foa Torres, *Phys. Rev. B* **97**, 121401 (2018).
- [85] S. Yao and Z. Wang, *Phys. Rev. Lett.* **121**, 086803 (2018).
- [86] S. Yao, F. Song, and Z. Wang, *Phys. Rev. Lett.* **121**, 136802 (2018).
- [87] F. K. Kunst, E. Edvardsson, J. C. Budich, and E. J. Bergholtz, *Phys. Rev. Lett.* **121**, 026808 (2018).
- [88] E. Edvardsson, F. K. Kunst, and E. J. Bergholtz, *Phys. Rev. B* **99**, 081302 (2019).
- [89] D. S. Borgnia, A. J. Kruchkov, and R.-J. Slager, *Phys. Rev. Lett.* **124**, 056802 (2020).
- [90] C. H. Lee and R. Thomale, *Phys. Rev. B* **99**, 201103 (2019).
- [91] K. Zhang, Z. Yang, and C. Fang, *Phys. Rev. Lett.* **125**, 126402 (2020).
- [92] N. Okuma, K. Kawabata, K. Shiozaki, and M. Sato, *Phys. Rev. Lett.* **124**, 086801 (2020).
- [93] N. Okuma and M. Sato, *Annual Review of Condensed Matter Physics* **14**, 83 (2023).
- [94] L. Xiao, T. Deng, K. Wang, G. Zhu, Z. Wang, W. Yi, and P. Xue, *Nature Physics* **16**, 761 (2020).
- [95] T. Helbig, T. Hofmann, S. Imhof, M. Abdelghany, T. Kiessling, L. W. Molenkamp, C. H. Lee, A. Szameit, M. Greiter, and R. Thomale, *Nature Physics* **16**, 747 (2020).
- [96] Q. Liang, D. Xie, Z. Dong, H. Li, H. Li, B. Gadway, W. Yi, and B. Yan, *Phys. Rev. Lett.* **129**, 070401 (2022).
- [97] T. Yoshida, T. Mizoguchi, and Y. Hatsugai, *Phys. Rev. Research* **2**, 022062 (2020).
- [98] R. Okugawa, R. Takahashi, and K. Yokomizo, *Phys. Rev. B* **102**, 241202 (2020).
- [99] K. Kawabata, M. Sato, and K. Shiozaki, *Phys. Rev. B* **102**, 205118 (2020).
- [100] Y. Fu and S. Wan, arXiv preprint arXiv:2008.09033 (2020).
- [101] N. Okuma and M. Sato, *Phys. Rev. Lett.* **123**, 097701 (2019).

- [102] F. Song, S. Yao, and Z. Wang, *Phys. Rev. Lett.* **123**, 170401 (2019).
- [103] T. Haga, M. Nakagawa, R. Hamazaki, and M. Ueda, *Phys. Rev. Lett.* **127**, 070402 (2021).
- [104] F. Yang, Q.-D. Jiang, and E. J. Bergholtz, *Phys. Rev. Res.* **4**, 023160 (2022).
- [105] G. Hwang and H. Obuse, arXiv preprint arXiv:2305.08548 (2023).
- [106] T. Tomita, S. Nakajima, I. Danshita, Y. Takasu, and Y. Takahashi, *Science Advances* **3**, e1701513 (2017).
- [107] T. Tomita, S. Nakajima, Y. Takasu, and Y. Takahashi, *Phys. Rev. A* **99**, 031601 (2019).
- [108] Y. Takasu, T. Yagami, Y. Ashida, R. Hamazaki, Y. Kuno, and Y. Takahashi, *Progress of Theoretical and Experimental Physics* **2020**, 12A110 (2020).
- [109] R. Ma, B. Saxberg, C. Owens, N. Leung, Y. Lu, J. Simon, and D. I. Schuster, *Nature* **566**, 51 (2019).
- [110] T. Yoshida, K. Kudo, and Y. Hatsugai, *Scientific Reports* **9**, 16895 (2019).
- [111] T. Yoshida, K. Kudo, H. Katsura, and Y. Hatsugai, *Phys. Rev. Research* **2**, 033428 (2020).
- [112] C.-X. Guo, X.-R. Wang, C. Wang, and S.-P. Kou, *Phys. Rev. B* **101**, 144439 (2020).
- [113] N. Matsumoto, K. Kawabata, Y. Ashida, S. Furukawa, and M. Ueda, *Phys. Rev. Lett.* **125**, 260601 (2020).
- [114] Q. Zhang, W.-T. Xu, Z.-Q. Wang, and G.-M. Zhang, *Communications Physics* **3**, 209 (2020).
- [115] C.-X. Guo, X.-R. Wang, and S.-P. Kou, *EPL (Europhysics Letters)* **131**, 27002 (2020).
- [116] H. Shackleton and M. S. Scheurer, *Phys. Rev. Research* **2**, 033022 (2020).
- [117] K. Yang, S. C. Morampudi, and E. J. Bergholtz, *Phys. Rev. Lett.* **126**, 077201 (2021).
- [118] Z. Wang, X.-D. Dai, H.-R. Wang, and Z. Wang, arXiv preprint arXiv:2306.12482 (2023).
- [119] D.-W. Zhang, Y.-L. Chen, G.-Q. Zhang, L.-J. Lang, Z. Li, and S.-L. Zhu, *Phys. Rev. B* **101**, 235150 (2020).
- [120] T. Liu, J. J. He, T. Yoshida, Z.-L. Xiang, and F. Nori, *Phys. Rev. B* **102**, 235151 (2020).
- [121] Z. Xu and S. Chen, *Phys. Rev. B* **102**, 035153 (2020).
- [122] L. Pan, X. Wang, X. Cui, and S. Chen, *Phys. Rev. A* **102**, 023306 (2020).
- [123] W. Xi, Z.-H. Zhang, Z.-C. Gu, and W.-Q. Chen, *Science Bulletin* **66**, 1731 (2021).
- [124] T. Yoshida and Y. Hatsugai, *Phys. Rev. B* **104**, 075106 (2021).
- [125] T. Yoshida and Y. Hatsugai, *Phys. Rev. B* **106**, 205147 (2022).
- [126] T. Yoshida and Y. Hatsugai, *Phys. Rev. B* **107**, 075118 (2023).
- [127] T. Orito and K.-I. Imura, *Phys. Rev. B* **105**, 024303 (2022).
- [128] R. Shen and C. H. Lee, *Communications Physics* **5**, 238 (2022).
- [129] S. Mu, C. H. Lee, L. Li, and J. Gong, *Phys. Rev. B* **102**, 081115 (2020).
- [130] C. H. Lee, *Phys. Rev. B* **104**, 195102 (2021).
- [131] S.-B. Zhang, M. M. Denner, T. c. v. Bzdušek, M. A. Sentef, and T. Neupert, *Phys. Rev. B* **106**, L121102 (2022).
- [132] K. Kawabata, K. Shiozaki, and S. Ryu, *Phys. Rev. B* **105**, 165137 (2022).
- [133] F. Alsallom, L. Herviou, O. V. Yazyev, and M. Brzezińska, *Phys. Rev. Res.* **4**, 033122 (2022).
- [134] W. N. Faugno and T. Ozawa, *Phys. Rev. Lett.* **129**, 180401 (2022).
- [135] S. Hamanaka, K. Yamamoto, and T. Yoshida, arXiv preprint arXiv:2305.19697 (2023).
- [136] S. Tsubota, H. Yang, Y. Akagi, and H. Katsura, *Phys. Rev. B* **105**, L201113 (2022).
- [137] S. Sayyad and J. L. Lado, *Phys. Rev. Res.* **5**, L022046 (2023).
- [138] G. Chen, F. Song, and J. L. Lado, *Phys. Rev. Lett.* **130**, 100401 (2023).
- [139] S. Sayyad, arXiv preprint arXiv:2306.14766 (2023).
- [140] S. Sayyad and J. L. Lado, arXiv preprint arXiv:2309.06303 (2023).
- [141] To be precise, “spin” denotes pseudo-spin because the system is bosonic. However, for simplicity, we denote it by “spin”.
- [142] The point-gap of the many-body Hamiltonian opens for $\det(\hat{H}_{[N_\uparrow, N_\downarrow]}(\theta_s) - E_{\text{ref}})$.
- [143] This is because the Hamiltonian (1) is decomposed into two bosonic Hatano-Nelson model where the hopping to the right (left) is larger than the other for $\sigma = \uparrow$ ($\sigma = \downarrow$).
- [144] Supplemental Material for details of the perturbation theory, detailed results of the bosonic Hubbard model.
- [145] It is known that when hopping integrals of the Hatano-Nelson model are real, all of the eigenvalues take real values, which can be seen by applying an imaginary gauge transformation (see Sec. S2 of Supplemental Material [144]). Combining this fact and realness of iJ_+ and iJ_- , we can see that all of the eigenvalues of the effective spin model (9) are purely imaginary.
- [146] L. Garbe, Y. Minoguchi, J. Huber, and P. Rabl, arXiv preprint arXiv:2301.11339 (2023).
- [147] Here, we note that the Mott skin effect is also observed for other subspaces of half-filling $N_\uparrow + N_\downarrow = L$. For instance, the Mott skin effect is observed for the subspace with $[N_\uparrow, N_\downarrow] = [2, 4]$ and $L = 6$ (see Sec. S5 of Supplemental Material [144]).
- [148] The results of eigenvalues are consistent with the results of perturbation theory, which can be seen by noting that the parameters of \hat{H}_{spin} take the following values: $(J_+, J_-) = (-0.1i, -0.001i)$ and $J_z(\frac{L}{4} - 1) + E_0 = -0.028i$ for $(t_+, t_-, V, U) = (-1, 0.1, 100, 20)$ and $L = 6$.
- [149] We note that post-selected real-time dynamics of open quantum systems are described by $i\partial_t|\Phi(t)\rangle = \hat{H}|\Phi(t)\rangle$ [48].
- [150] We note that Bloch oscillation is observed around the left edge ($j = 0$) as illustrated by the arrow in Fig. 3(a). This oscillation is due to the interference between skin modes whose time-evolution is given by $e^{-i\hat{H}t}|\Phi_m\rangle_{\text{R}} = e^{-iE_m t}|\Phi_m\rangle_{\text{R}}$.
- [151] B. H. Kim, J.-H. Han, and M. J. Park, arXiv preprint arXiv:2309.07894 (2023).

Supplemental Materials:
Non-Hermitian Mott Skin Effect

S1. DETAILS OF THE EFFECTIVE SPIN MODEL

A. Derivation of Equation (7)

Here, based on the second order perturbation theory, we derive the effective spin model [see Eq. (7)] for $V, U \gg t_+, t_-$. In the following, we impose PBC for the sake of simplicity.

Let us consider a Fock space where each site is occupied by a boson. For such a Fock space, the effective Hamiltonian can be written as

$$\begin{aligned}\hat{H}_{\text{ptb}} &= \hat{H}_{\text{ptb,RL}} + \hat{H}_{\text{ptb,LR}}, \\ \hat{H}_{\text{ptb,RL}} &= \sum_{j\sigma s} \hat{P} \left[t_{\text{R}\sigma} t_{\text{L}s} \hat{b}_{j+1\sigma}^\dagger \hat{b}_{j\sigma} \frac{1}{E_g - \hat{H}_{\text{int}}} \hat{b}_{j s}^\dagger \hat{b}_{j+1s} \right] \hat{P}, \\ \hat{H}_{\text{ptb,LR}} &= \sum_{j\sigma s} \hat{P} \left[t_{\text{L}\sigma} t_{\text{R}s} \hat{b}_{j\sigma}^\dagger \hat{b}_{j+1\sigma} \frac{1}{E_g - \hat{H}_{\text{int}}} \hat{b}_{j+1s}^\dagger \hat{b}_{j s} \right] \hat{P},\end{aligned}\tag{S1}$$

where \hat{P} is the projection operator of the Fock space where a boson occupies each site. The ground state energy E_g takes zero $E_g = \hat{P} \hat{H}_{\text{int}} \hat{P} = 0$.

By a straightforward calculation, we obtain

$$\begin{aligned}\hat{H}_{\text{ptb,RL}} &= -i \sum_{j\sigma} \frac{t_{\text{R}\sigma} t_{\text{L}\sigma}}{V} \hat{P} (\hat{n}_{j+1\sigma} \hat{n}_{j\sigma}) \hat{P} \\ &\quad -i \sum_{j\sigma} \frac{t_{\text{R}\sigma} t_{\text{L}\sigma}}{U} \hat{P} (\hat{n}_{j+1\sigma} \hat{n}_{j\bar{\sigma}}) \hat{P} \\ &\quad -i \sum_{j\sigma} \frac{t_{\text{R}\sigma} t_{\text{L}\bar{\sigma}}}{U} \hat{P} (\hat{b}_{j+1\sigma}^\dagger \hat{b}_{j+1\bar{\sigma}} \hat{b}_{j\bar{\sigma}}^\dagger \hat{b}_{j\sigma}) \hat{P},\end{aligned}\tag{S2}$$

where $\bar{\sigma}$ takes \downarrow (\uparrow) for $\sigma = \uparrow$ ($\sigma = \downarrow$).

By using the following relations

$$4\hat{S}_{j+1}^z \hat{S}_j^z + \hat{n}_{j+1} \hat{n}_j = 2(\hat{n}_{j+1\uparrow} \hat{n}_{j\uparrow} + \hat{n}_{j+1\downarrow} \hat{n}_{j\downarrow}),\tag{S3}$$

$$-4\hat{S}_{j+1}^z \hat{S}_j^z + \hat{n}_{j+1} \hat{n}_j = 2(\hat{n}_{j+1\uparrow} \hat{n}_{j\downarrow} + \hat{n}_{j+1\downarrow} \hat{n}_{j\uparrow}),\tag{S4}$$

we obtain

$$\begin{aligned}\hat{H}_{\text{ptb,RL}} &= \sum_j \left[-i \frac{t_+ t_-}{2V} \hat{P} (4\hat{S}_{j+1}^z \hat{S}_j^z + \hat{n}_{j+1} \hat{n}_j) \hat{P} \right. \\ &\quad \left. -i \frac{t_+ t_-}{2U} \hat{P} (-4\hat{S}_{j+1}^z \hat{S}_j^z + \hat{n}_{j+1} \hat{n}_j) \hat{P} \right. \\ &\quad \left. -i \frac{t_+^2}{U} \hat{P} (\hat{S}_{j+1}^+ \hat{S}_j^-) \hat{P} - i \frac{t_-^2}{U} \hat{P} (\hat{S}_{j+1}^- \hat{S}_j^+) \hat{P} \right],\end{aligned}\tag{S5}$$

where we have also chosen the parameters as $(t_{\text{R}\uparrow}, t_{\text{R}\downarrow}) = (t_+, t_-)$ and $(t_{\text{L}\uparrow}, t_{\text{L}\downarrow}) = (t_-, t_+)$.

In a similar way, we obtain

$$\begin{aligned} \hat{H}_{\text{ptb,LR}} = & \sum_j \left[-i \frac{t_+ t_-}{2V} \hat{P} \left(4 \hat{S}_{j+1}^z \hat{S}_j^z + \hat{n}_{j+1} \hat{n}_j \right) \hat{P} \right. \\ & - i \frac{t_+ t_-}{2U} \hat{P} \left(-4 \hat{S}_{j+1}^z \hat{S}_j^z + \hat{n}_{j+1} \hat{n}_j \right) \hat{P} \\ & \left. - i \hat{P} \left(\frac{t_+^2}{U} \hat{S}_{j+1}^+ \hat{S}_j^- + \frac{t_-^2}{U} \hat{S}_{j+1}^- \hat{S}_j^+ \right) \hat{P} \right]. \end{aligned} \quad (\text{S6})$$

Therefore, the effective Hamiltonian is obtained as

$$\hat{H}_{\text{ptb}} = \sum_j \left[J_+ \hat{S}_{j+1}^+ \hat{S}_j^- + J_- \hat{S}_{j+1}^- \hat{S}_j^+ + J_z \hat{S}_{j+1}^z \hat{S}_j^z \right] + E_0, \quad (\text{S7})$$

with

$$J_+ = -2i \frac{t_+^2}{U}, \quad (\text{S8})$$

$$J_- = -2i \frac{t_-^2}{U}, \quad (\text{S9})$$

$$J_z = -4it_+ t_- \left(\frac{1}{V} - \frac{1}{U} \right), \quad (\text{S10})$$

$$E_0 = -4it_+ t_- L \left(\frac{1}{V} + \frac{1}{U} \right). \quad (\text{S11})$$

Equation (S7) corresponds to the spin model [Eq. (7)].

Under twisted boundary conditions, the following replacement results in the effective Hamiltonian $\hat{H}_{\text{spin}}(\theta_s)$:

$$\hat{S}_0^+ \hat{S}_{L-1}^- \rightarrow e^{2i\theta} \hat{S}_0^+ \hat{S}_{L-1}^-, \quad (\text{S12})$$

$$\hat{S}_0^- \hat{S}_{L-1}^+ \rightarrow e^{-2i\theta} \hat{S}_0^- \hat{S}_{L-1}^+. \quad (\text{S13})$$

Therefore, we obtain the spin model shown in Eq. (7).

B. Derivation of Eq. (9)

Applying the Jordan-Wigner transformation to the effective spin model [see Eq. (7)] yields the spinless fermion model [see Eq. (8)].

With the Jordan-Wigner transformation, \hat{S}_j^+ and \hat{S}_j^z are rewritten as

$$\hat{S}_j^+ = e^{i\pi \hat{N}_j^<} \hat{f}_j^\dagger, \quad (\text{S14})$$

$$\hat{S}_j^z = \left(\hat{n}_j^f - \frac{1}{2} \right), \quad (\text{S15})$$

with creation (annihilation) operators of spinless fermions \hat{f}_j^\dagger (\hat{f}_j). Here, the operators are defined as $\hat{N}_j^< = \sum_{i=0}^{j-1} \hat{n}_i^f$, $\hat{N}^f = \sum_j \hat{n}_j^f$, and $\hat{n}_j^f = \hat{f}_j^\dagger \hat{f}_j$.

Thus, each term of the spin model is transformed as follows: for $0 \leq j < L-1$,

$$\hat{S}_{j+1}^+ \hat{S}_j^- = \hat{f}_{j+1}^\dagger \hat{f}_j, \quad (\text{S16})$$

$$\hat{S}_{j+1}^- \hat{S}_j^+ = \hat{f}_j^\dagger \hat{f}_{j+1}, \quad (\text{S17})$$

and for $j = L - 1$,

$$\begin{aligned}\hat{S}_{j+1}^+ \hat{S}_j^- &= \hat{f}_0^\dagger e^{i\pi \hat{N}_{L-1}^<} \hat{f}_{L-1} \\ &= \hat{f}_0^\dagger e^{i\pi(\hat{N}^f + \hat{n}_{L-1}^f)} \hat{f}_{L-1} \\ &= -e^{i\pi \hat{N}^f} \hat{f}_0^\dagger e^{i\pi \hat{n}_{L-1}^f} \hat{f}_{L-1} \\ &= -e^{i\pi \hat{N}^f} \hat{f}_0^\dagger \hat{f}_{L-1},\end{aligned}\tag{S18}$$

$$\begin{aligned}\hat{S}_{j+1}^- \hat{S}_j^+ &= \hat{f}_0 e^{i\pi \hat{N}_{L-1}^<} \hat{f}_{L-1}^\dagger \\ &= \hat{f}_0 e^{i\pi(\hat{N}^f + \hat{n}_{L-1}^f)} \hat{f}_{L-1}^\dagger \\ &= -e^{i\pi \hat{N}^f} \hat{f}_{L-1}^\dagger \hat{f}_0.\end{aligned}\tag{S19}$$

In a similar way, we obtain

$$\hat{S}_{j+1}^z \hat{S}_j^z = (\hat{n}_{j+1}^f - \frac{1}{2})(\hat{n}_j^f - \frac{1}{2}),\tag{S20}$$

for $0 \leq j \leq L - 1$.

Therefore, the effective spin model is rewritten as

$$\begin{aligned}\hat{H}_{\text{spin}}(\theta) &= \sum_{j=0}^{L-2} \left(J_+ \hat{f}_{j+1}^\dagger \hat{f}_j + J_- \hat{f}_j^\dagger \hat{f}_{j+1} \right) \\ &\quad - (-1)^{\hat{N}^f} \left(J_+ e^{2i\theta_s} \hat{f}_0^\dagger \hat{f}_{L-1} + J_- e^{-2i\theta_s} \hat{f}_{L-1}^\dagger \hat{f}_0 \right) \\ &\quad + J_z \sum_{j=0}^{L-1} \hat{n}_{j+1}^f \hat{n}_j^f - J_z \left(\hat{N}^f - \frac{L}{4} \right) + E_0.\end{aligned}\tag{S21}$$

In particular, for the Fock space with $S^z = 1 - \frac{L}{2}$ (i.e., $[N_\uparrow, N_\downarrow] = [1, L - 1]$), there exists only one fermion created by \hat{f}_j^\dagger . In this case, the following terms are simplified as

$$\sum_{j=0}^{L-1} \hat{n}_{j+1}^f \hat{n}_j^f \rightarrow 0\tag{S22}$$

$$\hat{N}^f - \frac{L}{4} \rightarrow 1 - \frac{L}{4}.\tag{S23}$$

Therefore, we obtain Eq. (9) for the subspace with $S^z = 1 - \frac{L}{2}$.

S2. PROPERTIES OF THE ONE-BODY HAMILTONIAN

By analyzing the first quantized Hamiltonian, we see that the system shows the non-Hermitian skin effect at the non-interacting case. The Hamiltonian (2) is written as

$$\hat{H}_0 = \sum_k h_\sigma(k) \hat{b}_{k\sigma}^\dagger \hat{b}_{k\sigma}\tag{S24}$$

with $\hat{b}_{k\sigma}^\dagger = \frac{1}{\sqrt{L}} \sum_j e^{-ikj} \hat{b}_{j\sigma}^\dagger$ and $0 \leq k < 2\pi$. Here, we have imposed PBC. The first quantized Hamiltonian $h_\uparrow(k)$ and $h_\downarrow(k)$ are written as $h_\uparrow(k) = t_+ e^{ik} + t_- e^{-ik}$ and $h_\downarrow(k) = t_- e^{ik} + t_+ e^{-ik}$, respectively.

Now, we introduce the spin winding number w_s characterizing the point-gap topology of the first quantized Hamiltonian $h(\mathbf{k}) = \begin{pmatrix} h_\uparrow(\mathbf{k}) & 0 \\ 0 & h_\downarrow(\mathbf{k}) \end{pmatrix}$. The spin winding number w_s is defined as

$$w_s(\epsilon_{\text{ref}}) = \int_0^{2\pi} \frac{dk}{2\pi i} \partial_k \text{tr} [s_z \log(h(k) - \epsilon_{\text{ref}} \mathbb{1}_{2 \times 2})],\tag{S25}$$

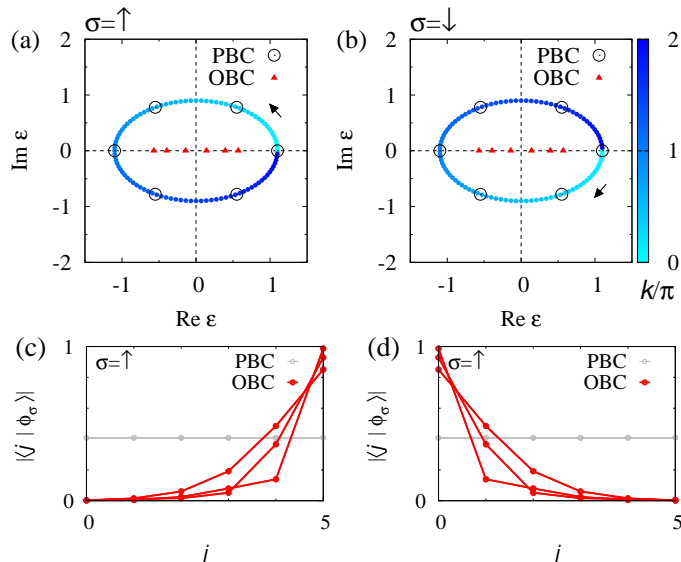


FIG. S1. (a) [(b)]: Eigenvalues of the one-body Hamiltonian for $\sigma = \uparrow$ [$\sigma = \downarrow$]. Open circles (closed triangle) denote the data under PBC (OBC) for $L = 6$. Closed circles denote the data under PBC for $L = 100$. The color of the closed circles represent the momentum k . (c) [(d)]: Amplitude of the right eigenvectors for $\sigma = \uparrow$ [$\sigma = \downarrow$]. The gray (red) lines denote the data under PBC (OBC) for $L = 6$.

with $\epsilon_{\text{ref}} \in \mathbb{C}$, $\mathbf{1}_{2 \times 2}$ being the 2×2 identity matrix, and $s^z = \frac{1}{2} \begin{pmatrix} 1 & 0 \\ 0 & -1 \end{pmatrix}$. The derivative with respect to k is denoted by ∂_k .

Figures S1(a) and S1(b) display the eigenvalues of the one-body Hamiltonian $\epsilon_{k\sigma} = h_\sigma(k)$ under PBC. This figure indicates that the spin winding number takes 1 for $\epsilon_{\text{ref}} = 0$.

This non-trivial point-gap topology induces extreme sensitivity of eigenvalues and eigenstates to the presence or absence of the boundaries. Figures S1(a) and S1(b) indicate that the eigenvalues are aligned on the real axis under OBC in contrast to the case of PBC. Correspondingly, the system under OBC exhibits the skin modes localized around the boundaries [see Figs. S1(c) and S1(d)].

The above results indicate that the first quantized Hamiltonian shows the non-Hermitian skin effect. We finish this part with a remark on the realness of eigenvalues under OBC which can be understood by applying an imaginary gauge transformation. Introducing operators

$$\bar{a}_j = e^{-\phi j} \hat{c}_j^\dagger, \quad (\text{S26})$$

$$\hat{a}_j = e^{\phi j} \hat{c}_j, \quad (\text{S27})$$

we can rewrite the non-interacting Hamiltonian \hat{H}_0 under OBC

$$\hat{H}_0 = -t_a \sum_{j=0, \dots, L-2} [\bar{a}_{j+1\sigma} \hat{a}_{j\sigma} + \bar{a}_{j\sigma} \hat{a}_{j+1\sigma}]. \quad (\text{S28})$$

with $t_a = \sqrt{t_R t_L}$ and $\phi = \frac{1}{2} \ln \left(\frac{t_L}{t_R} \right)$. Here \bar{a}_j and \hat{a}_j satisfy the anti-commutation relation $\{\hat{a}_i, \bar{a}_j\} = \delta_{ij}$. Equation (S28) can be regarded as the Hermitian Hamiltonian. Thus, all of the eigenvalues are real.

S3. DETAILS OF COMPUTATION OF W_s

Let us discuss the computation of W_s in details. Under twisted boundary conditions, the non-interacting Hamiltonian is written as

$$\hat{H}_0(\theta_s) = \sum_{\sigma=\uparrow,\downarrow} \left[\sum_{j=0}^{L-2} \left(-t_{R\sigma} \hat{b}_{j+1\sigma}^\dagger \hat{b}_{j\sigma} - t_{L\sigma} \hat{b}_{j\sigma}^\dagger \hat{b}_{j+1\sigma} \right) - t_{R\sigma} e^{i\theta_s} \hat{b}_{0\sigma}^\dagger \hat{b}_{L-1\sigma} - t_{L\sigma} e^{i\theta_s} \hat{b}_{L-1\sigma}^\dagger \hat{b}_{0\sigma} \right] \quad (\text{S29})$$

with $\theta_\uparrow = \theta_s$ and $\theta_\downarrow = -\theta_s$. As mentioned below Eq. (2), $t_{R\sigma}$ and $t_{L\sigma}$ are chosen as $t_{R\uparrow} = t_{L\downarrow} = t_+$ and $t_{L\uparrow} = t_{R\downarrow} = t_-$.

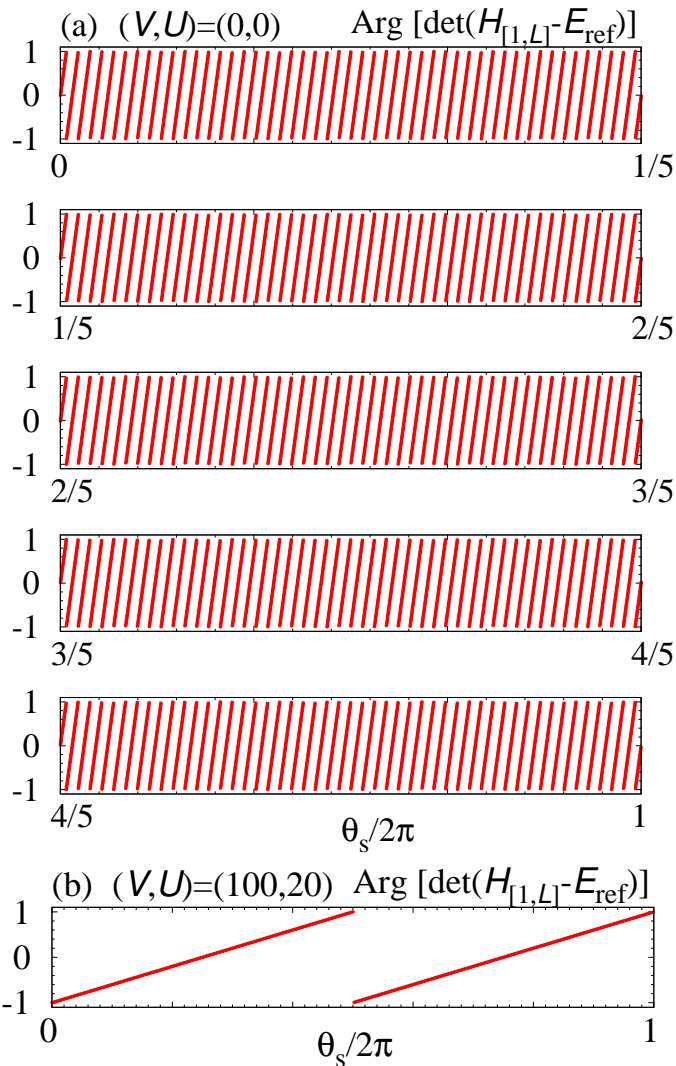


FIG. S2. Argument $\text{Arg}[\det(\hat{H}_{[1,L-1]} - E_{\text{ref}})]$ as functions of θ_s with $E_{\text{ref}} = -0.01i$. Panel (a) [(b)] displays the data for $(V,U) = (0,0)$ [(100,20)].

Equation (6) indicates that the many-body winding number W_s can be extracted from θ_s dependence of the argument, $\text{Arg}[\det(\hat{H}_{[1,L-1]} - E_{\text{ref}})]$. Figure S2(a) displays the argument as a function of θ for $(V,U) = (0,0)$ and $E_{\text{ref}} = -0.01i$. This figure indicates that the winding number takes $W_s = 245$ for $E_{\text{ref}} = -0.01i$ in the non-interacting case. Figure S2(b) displays the argument as a function of θ for $(V,U) = (100,20)$ and $E_{\text{ref}} = -0.01i$. This figure indicates that the winding number takes $W_s = 2$ for $E_{\text{ref}} = -0.01i$ for the correlated case.

S4. EXPECTATION VALUES FOR PBC

We provide the expectation values under PBC. Under PBC, the expectation values $\langle \hat{n}_j \rangle$ and $\langle \hat{S}_j^z \rangle$ are homogeneous for the non-interacting case (see Fig. S3),

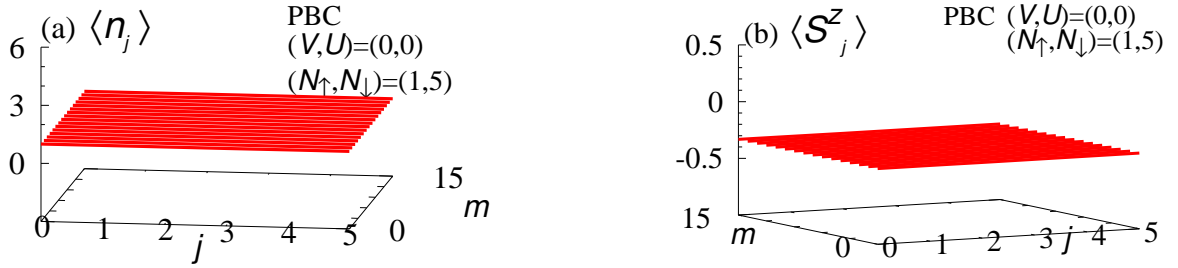


FIG. S3. The expectation values for $(V, U) = (0, 0)$ under PBC. Panel (a) [(b)] displays $\langle \hat{n}_j \rangle$ [$\langle \hat{S}_j^z \rangle$]. These data are obtained for $(t_+, t_-) = (1, 0.1)$ and $L = 6$. These figures are plotted in a similar way as Figs. 1(c) and 1(d).

These properties do not change even in the presence of the interactions. Figure S4 displays the expectation values $\langle \hat{n}_j \rangle$ and $\langle \hat{S}_j^z \rangle$ under PBC for $(V, U) = (100, 20)$.

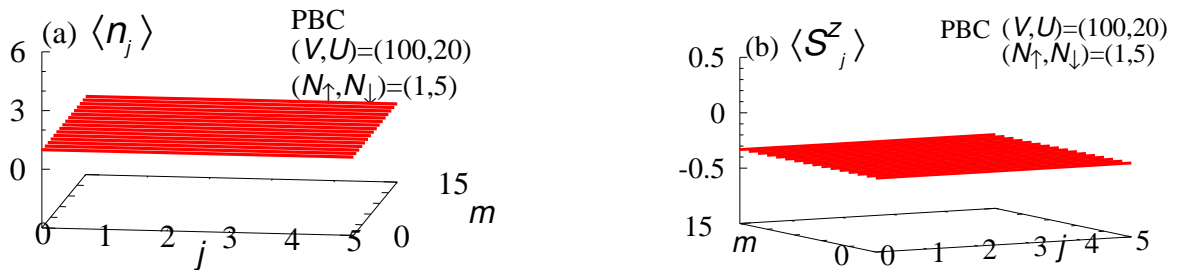


FIG. S4. The expectation values for $(V, U) = (100, 20)$ under PBC. Panel (a) [(b)] displays $\langle \hat{n}_j \rangle$ [$\langle \hat{S}_j^z \rangle$]. These data are obtained for $(t_+, t_-) = (1, 0.1)$ and $L = 6$. These figures are plotted in a similar way as Figs. 2(c) and 2(d).

S5. RESULTS FOR $(N_\uparrow, N_\downarrow) = (2, 4)$

Here, we provide the results for subspace with $(N_\uparrow, N_\downarrow) = (2, 4)$ and $L = 6$ which indicates that the Mott skin effect is still observed.

Let us start with the non-interacting case where the ordinary non-Hermitian skin effect is observed. Specifically, under PBC, the expectation values $\langle \hat{n}_j \rangle$ and $\langle \hat{S}_j^z \rangle$ are homogeneous [see Figs. S5(a) and S5(b)]. Imposing OBC results in the localization of eigenstates which is reflected in both expectation values $\langle \hat{n}_j \rangle$ and $\langle \hat{S}_j^z \rangle$ [see Figs. S5(c) and S5(d)].

In contrast to the non-interacting case, for $(V, U) = (100, 20)$, the emergence of the skin modes is observed only in the spin degree of freedom. Firstly, we note that under PBC, the expectation values $\langle \hat{n}_j \rangle$ and $\langle \hat{S}_j^z \rangle$ are homogeneous [see Figs. S6(a) and S6(b)]. Imposing OBC results in localization in the spin degree of freedom although such localization is not observed in the charge degree of freedom [see Figs. S6(c) and S6(d)].

The above results indicate that the Mott skin effect is observed even for the subspace with $(N_\uparrow, N_\downarrow) = (2, 4)$ and $L = 6$.

S6. TIME-EVOLUTION UNDER PBC

We discuss the time-evolution of the expectation values $\langle \hat{n}_j(t) \rangle$ and $\langle \hat{S}_j^z(t) \rangle$ under PBC. In a similar way to the case of OBC, we compute the expectation values $\langle \hat{n}_j(t) \rangle$ and $\langle \hat{S}_j^z(t) \rangle$ [see Eq. (11)]. The initial state is chosen so that all the bosons occupy site $j = 0$.

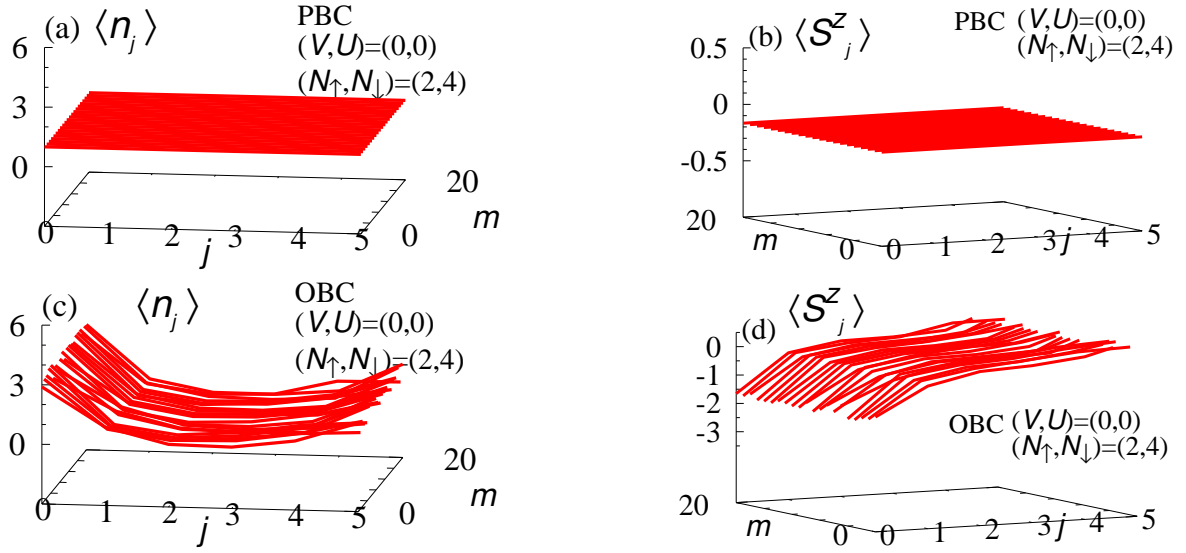


FIG. S5. The expectation values for the subspace with $(N_\uparrow, N_\downarrow) = (2, 4)$ and for $(V, U) = (0, 0)$. Panels (a) and (b) [(c) and (d)] are data under PBC. Panels (a) and (c) [(b) and (d)] display $\langle \hat{n}_j \rangle$ [$\langle \hat{S}_j^z \rangle$]. These figures are plotted in a similar way as Figs. 1(c) and 1(d). The data are obtained for $(t_+, t_-) = (1, 0.1)$ and $L = 6$.

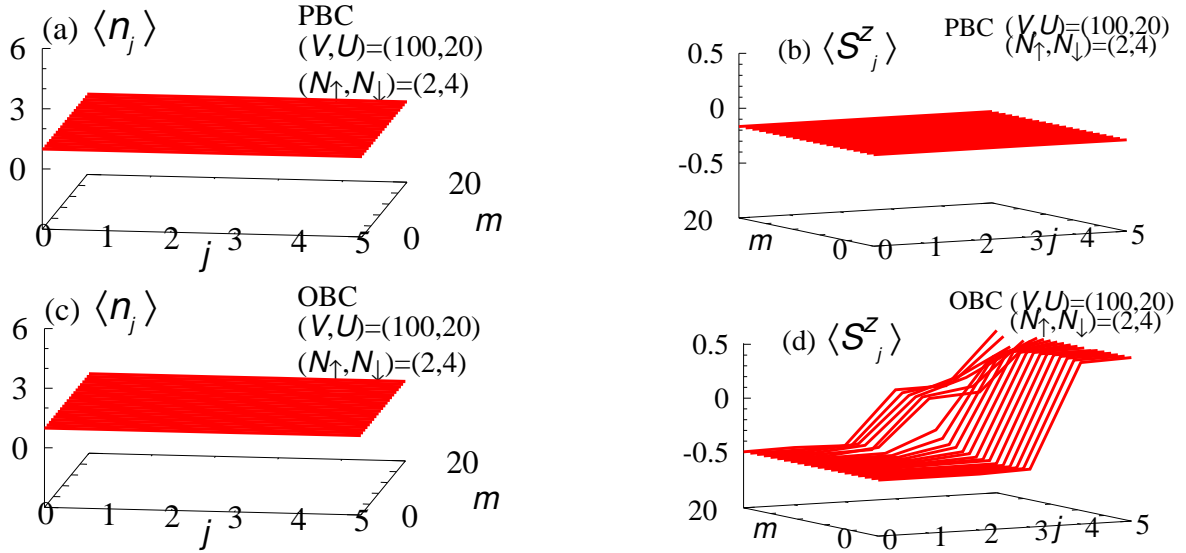


FIG. S6. The expectation values for the subspace with $(N_\uparrow, N_\downarrow) = (2, 4)$ and for $(V, U) = (100, 20)$. Panels (a) and (b) [(c) and (d)] are data under PBC. Panels (a) and (c) [(b) and (d)] display $\langle \hat{n}_j \rangle$ [$\langle \hat{S}_j^z \rangle$]. These figures are plotted in a similar way as Figs. 1(c) and 1(d). The data are obtained for $(t_+, t_-) = (1, 0.1)$ and $L = 6$.

Figures S7(a) and S7(b) display the data for the non-interacting case. In contrast to the case of OBC, bosons do not localize around the left edge $j = 0$ due to the absence of the skin modes. In addition, the bosons propagate to left, which is attributed to the fact that the eigenstates with the longest lifetime τ ($\tau \sim 1/\text{Im}E$) are composed of bosons propagating to left.

Figures S7(c) and S7(d) display the data for $(V, U) = (100, 20)$. In this case, increasing time t , the expectation values $\langle \hat{n}_j(t) \rangle$ and $\langle \hat{S}_j^z(t) \rangle$ become homogeneous. This is because the eigenstate with the longest lifetime τ ($\tau \sim 1/\text{Im}E$) is the state described by a fermion with zero momentum in terms of the effective fermion model (9).

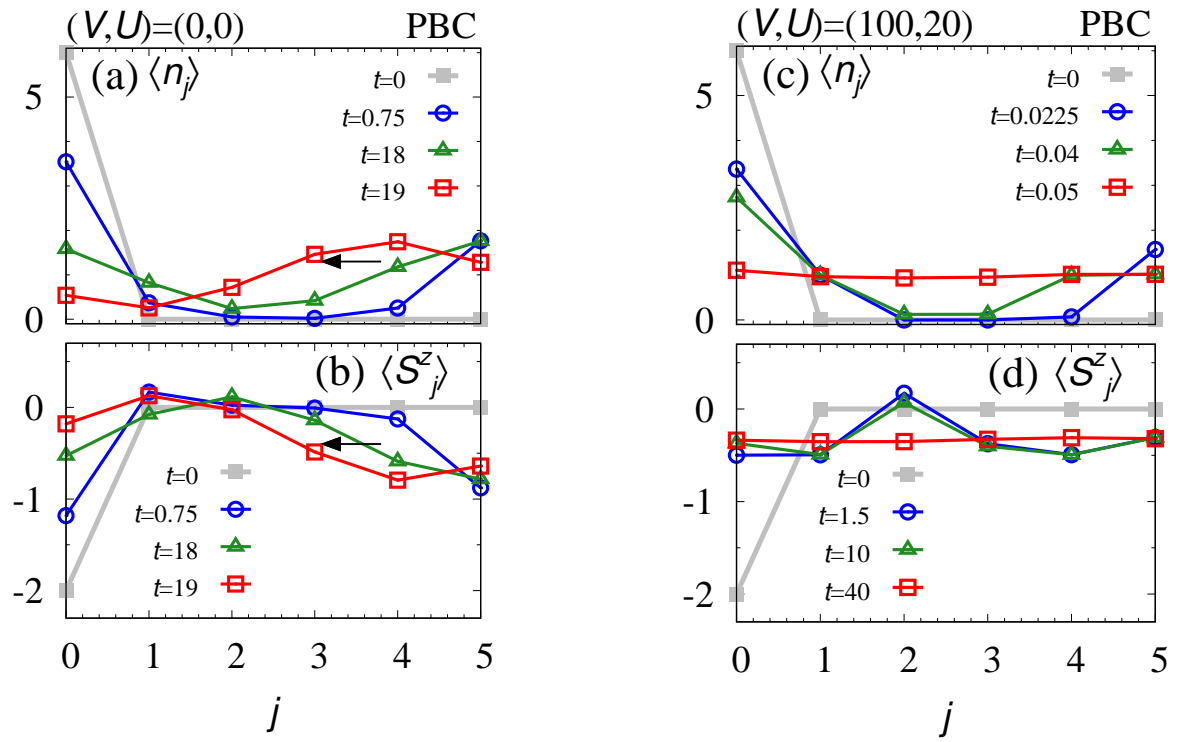


FIG. S7. The time-evolution of the expectation values $\langle \hat{n}_j(t) \rangle$ and $\langle \hat{S}_j^z(t) \rangle$ under PBC [see Eq. (11)] These figures are plotted in a similar way to Fig. 3 These data are obtained for $(t_+, t_-) = (1, 0.1)$ and $L = 6$.